Supplement of Atmos. Chem. Phys., 22, 12827–12855, 2022
https://doi.org/10.5194/acp-22-12827-2022-supplement


Atmospheric Chemistry and Physics
Open Access
EGU

*Supplement of*

# Ozone, DNA-active UV radiation, and cloud changes for the near-global mean and at high latitudes due to enhanced greenhouse gas concentrations

**Kostas Eleftheratos et al.**

*Correspondence to:* Kostas Eleftheratos (kelef@geol.uoa.gr)

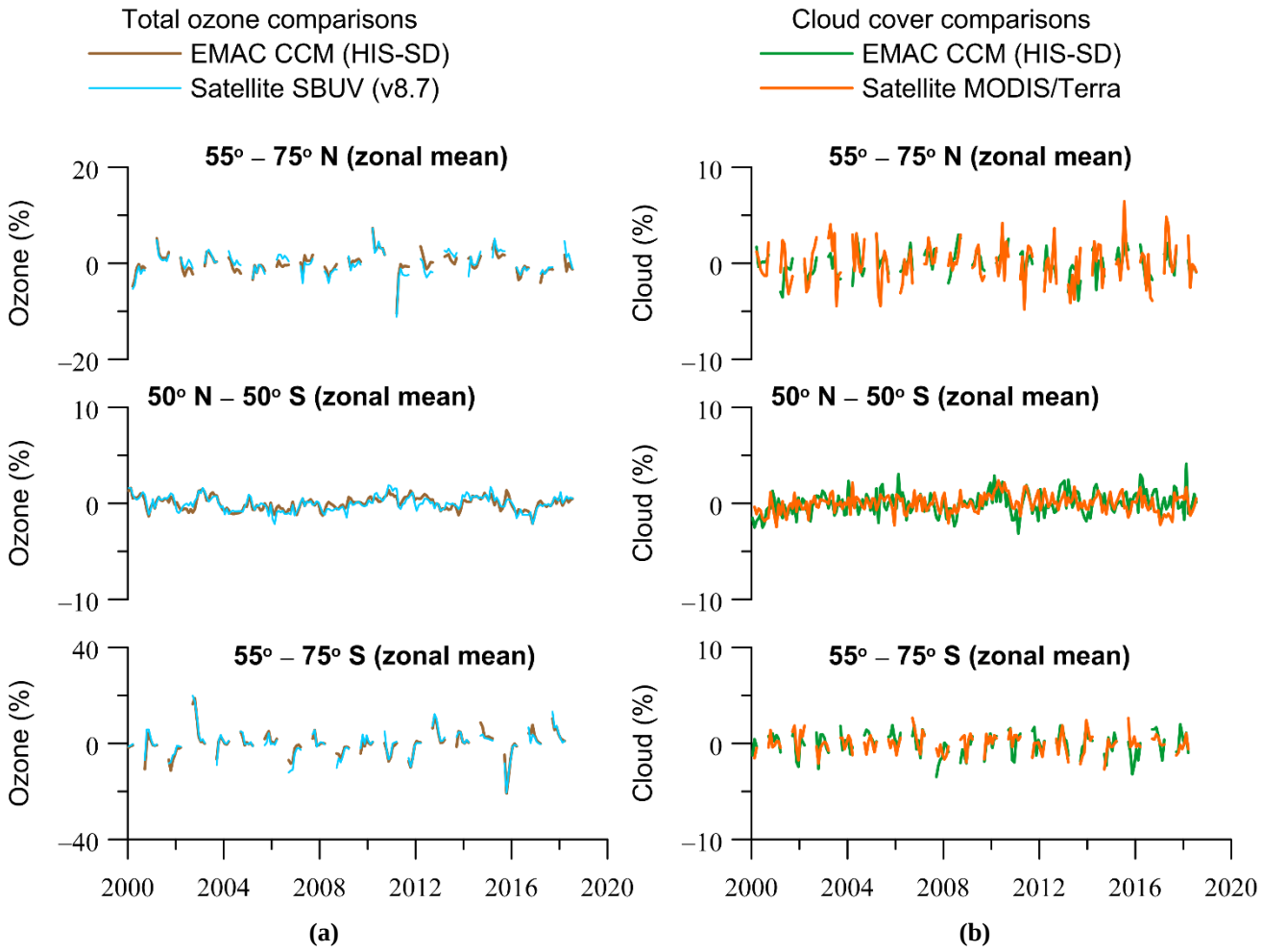


**Figure S1. (a)** Comparison of zonally averaged ozone column from model simulations and satellite measurements for the northern high latitudes (55°–75° N) (upper panel), the near-global mean (50° N–50° S) (middle panel) and the southern high latitudes (55°–75° S) (lower panel). **(b)** Same as **(a)** but for zonally averaged cloud cover. The y-axes show monthly de-seasonalized anomalies (in %) relative to the long-term monthly mean (2000–2018). Shown are monthly anomalies from March to September for the northern high latitudes, and from September to March for the southern high latitudes. For 50° N–50° S, we present all months.

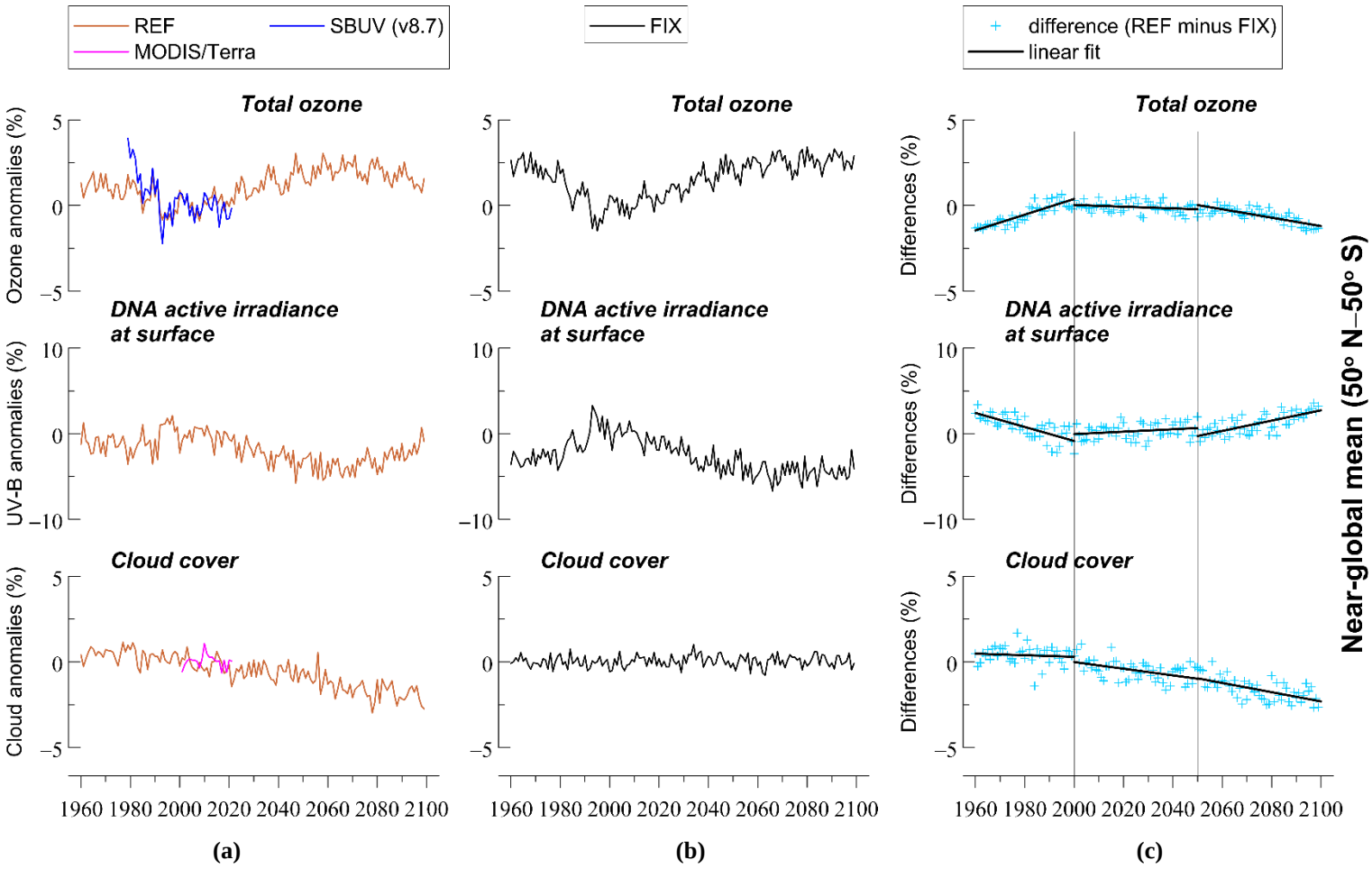


**Figure S2.** Changes in zonal mean total ozone, zonal mean DNA active irradiance and zonal mean cloud cover for the near global mean (50° N – 50° S), based on simulations with increasing and fixed GHGs mixing ratios. **(a)** REF is the simulation with increasing GHGs according to RCP-6.0. **(b)** FIX is the simulation with fixed GHGs emissions at 1960 levels. **(c)** Difference between the two model simulations, indicating the impact of increasing GHGs. The y-axes in (a) and (b) show yearly averaged data (in %) calculated from de-seasonalized monthly data. The monthly data were de-seasonalized relative to the long-term monthly mean (1990–2019) and were expressed in %. For 50° N–50° S we used all months to calculate the annual average.

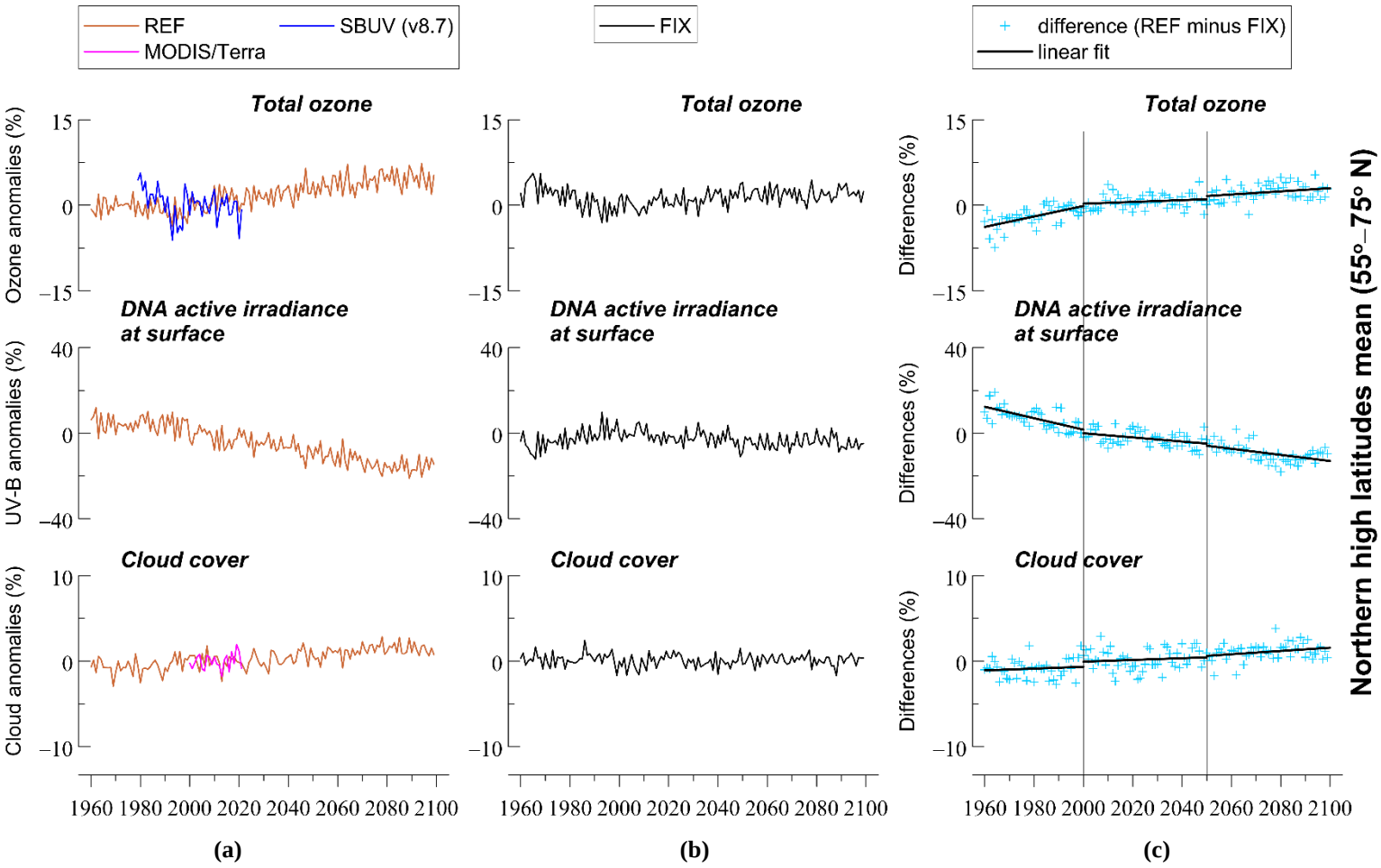


**Figure S3.** Same as Figure S2 but for northern high latitudes (55° – 75° N). The y-axes in (a) and (b) show yearly averaged data (in %) calculated from de-seasonalized monthly data. For the northern high latitudes, the annual average refers to the average of monthly anomalies from March to September.

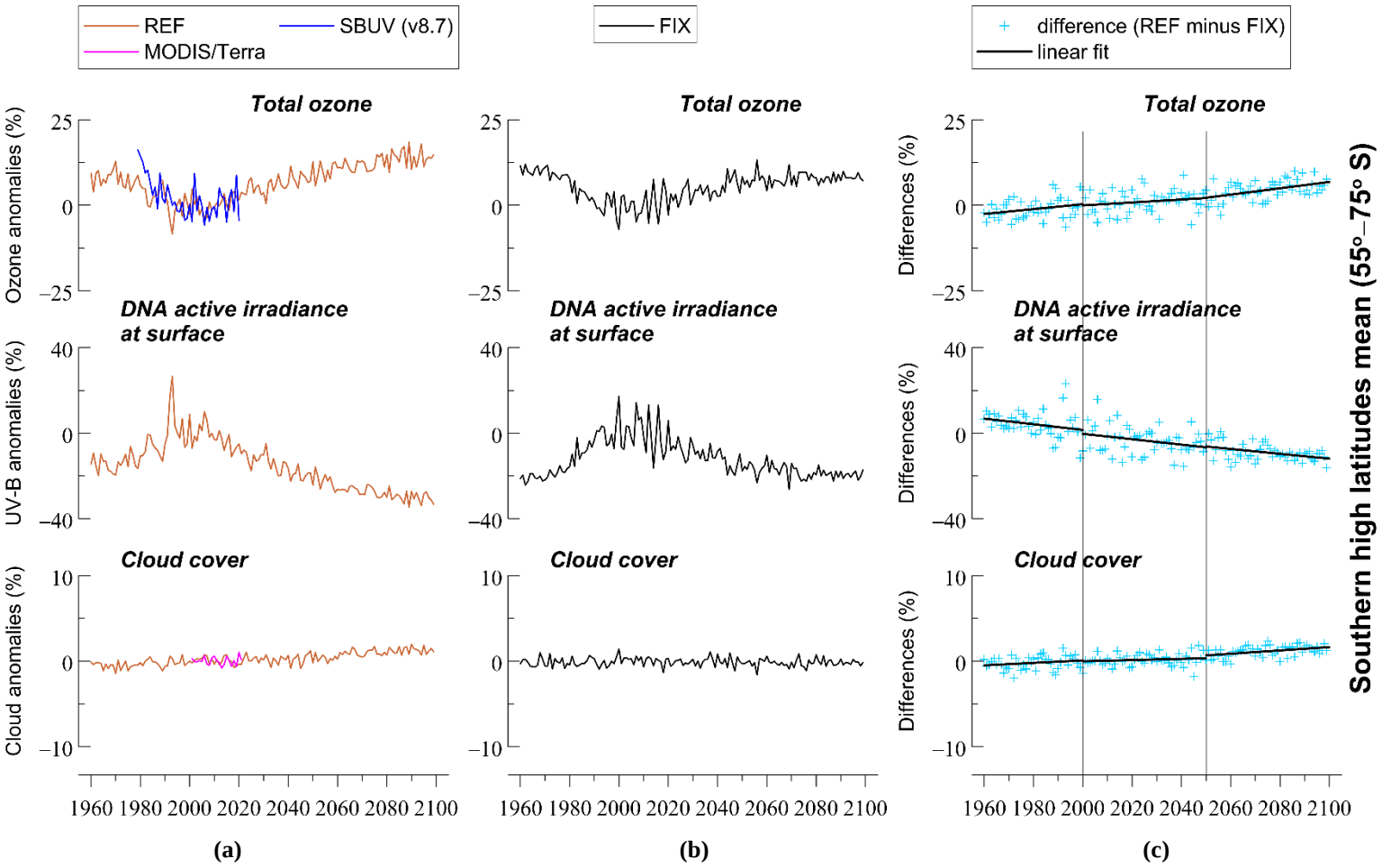


**Figure S4.** Same as Figure S2 but for southern high latitudes (55° – 75° S). The y-axes in (a) and (b) show yearly averaged data (in %) calculated from de-seasonalized monthly data. For the southern high latitudes, the annual average refers to the average of monthly anomalies from September to March.

**A note on the differences between the variability of DNA weighted irradiance from the model simulations and the corresponding measurements at some stations.**

The main reason for these differences in the variability of the DNA weighted irradiances (see figures below) is that we compare averages for 3° x 3° pixels (model simulations) with measurements performed at specific sites (representing narrow areas in the corresponding pixels). Thus, environmental features within the model pixel – that do not affect the station where measurements are performed – may lead to increased variability for the model with respect to the station. For example, the sites of Aosta, Lauder and Ushuaia are surrounded by very high mountains where surface albedo varies significantly in the year and affects strongly the levels of UV irradiance. The measurement sites however are at lower altitudes and changes in surface albedo do not affect strongly the levels of surface UV irradiance. In other sites (e.g., Villeneuve d'Ascq) environmental conditions are possibly less variable with respect to the average conditions in the pixel wherein they belong. Other sites (e.g., Summit, Thessaloniki, Boulder, Mauna Loa, or Alice Springs) are possibly more representative for the average conditions in the pixels wherein they belong. For Athens, the most possible explanation for the much higher measured UV relative to the UV simulated by the model in 2011 – 2014 is again that the model cannot accurately capture changes in air quality (e.g., aerosols, tropospheric ozone etc.) at the city since it represents a much wider area. We were not able to find aerosol optical properties in the UV for the same period for the site in order to verify our assumption but we intend to further investigate these differences in the future.

**A note on the differences between cloud cover from Modis/Terra and the model simulations at some stations.**

It would be nice if we obtained good model – satellite correlations from all datasets. We would have perfect model simulations and perfect satellite measurements at all locations. Frankly speaking, we cannot say which of the two datasets is responsible for the smaller agreement at some stations or if both are. But statistically speaking, we find that the majority of the stations (13 of 20 stations) show medium to good correlations (between 0.5 and 0.7), 5 stations show small to medium correlations (between 0.3 and 0.5), and only 2 stations show no correlation. The stations that show no correlation are Summit and South Pole. Both stations are high-altitude sites located at high latitudes with year-round snow cover and albedos of larger than 0.95. Multiple scattering between the surface and clouds greatly reduces cloud effects (Nichol et al., 2003). Mauna Loa (MLO) is also a high-altitude site. MLO is interesting, not only because it is also at high altitude, but because there are often clouds below the station, which enhance downwelling radiation similar to the effect of high albedo. Both in Antarctica and MLO, UV radiation is scattered up either by snow or a cloud layer, and then Rayleigh-scattered down to increase downwelling irradiance. However, we find that the correlation is 0.592 for the cloud case in MLO, suggesting that other contributing processes might account for somewhat successful cloud simulations in the EMAC model which would require further investigation. The stations with small to medium correlations (between 0.3 and 0.5) are Haute Provence, Athens, Lauder, Ushuaia and Palmer. We remind that all correlations were derived from de-seasonalized data, i.e. data after removing the mean seasonal cycle

of the period 2000-2018. This was performed because we wanted to evaluate the long-term variability of cloud cover and not its seasonal cycle.

## Reference

Nichol, S. E., Pfister, G., Bodeker, G. E., McKenzie, R. L., Wood, S. W., and Bernhard, G.: Moderation of cloud reduction of UV in the Antarctic due to high surface albedo, J. Applied Meteorology, 42, 1174–1183, DOI: https://doi.org/10.1175/1520-0450(2003)042<1174:MOCROU>2.0.CO;2, 2003.

**Table S1.** Statistics of correlations between simulated (EMAC CCM "specified dynamics" simulation SC1SD-base-02, referred as HIS-SD) and observed (ground-based) DNA active irradiance data after removing variability related to the seasonal cycle. Stations are listed from north to south.

| Station | Latitude | Correlation | Intercept (%) | Slope | Error | t-value | p-value | RMSE | N |
|---|---|---|---|---|---|---|---|---|---|
| Summit, Greenland | 72.58 | 0.70942 | -0.63182 | 0.75691 | 0.08109 | 9.33455 | <0.0001 | 8.41455 | 88 |
| Barrow, AK, United States | 71.32 | 0.34199 | 0.23804 | 0.68041 | 0.18074 | 3.76456 | 2.72957E-4 | 21.2041 | 109 |
| Sodankylä, Finland | 67.37 | 0.57099 | -1.43606 | 1.38698 | 0.17765 | 7.80726 | <0.0001 | 26.31277 | 128 |
| Villeneuve d'Ascq, France | 50.61 | 0.69524 | -0.7477 | 0.87007 | 0.07089 | 12.27297 | <0.0001 | 15.40379 | 163 |
| Groß-Enzersdorf, Austria | 48.20 | 0.58206 | -1.04209 | 0.64811 | 0.06711 | 9.65676 | <0.0001 | 15.37886 | 184 |
| Zugspitze, Germany | 47.42 | 0.2659 | 1.13542 | 0.2448 | 0.1281 | 1.91101 | 0.06198 | 14.8664 | 50 |
| Hoher Sonnblick, Austria | 47.05 | 0.67287 | 1.11524 | 0.94558 | 0.07542 | 12.53774 | <0.0001 | 13.93815 | 192 |
| Aosta, Italy | 45.74 | 0.67091 | -1.23967 | 1.33004 | 0.14016 | 9.48924 | <0.0001 | 14.76364 | 112 |
| Observatoire de Haute Provence, France | 43.94 | 0.57419 | -2.10876 | 0.72899 | 0.10447 | 6.97814 | <0.0001 | 15.51005 | 101 |
| Thessaloniki, Greece | 40.63 | 0.61157 | -0.65425 | 0.76343 | 0.06984 | 10.93159 | <0.0001 | 11.43093 | 202 |
| Boulder, CO, United States | 39.99 | 0.74751 | 0.19874 | 0.67683 | 0.0474 | 14.2792 | <0.0001 | 7.36597 | 163 |
| Athens, Greece | 37.99 | 0.46825 | -1.20784 | 0.31889 | 0.05141 | 6.20271 | <0.0001 | 7.87145 | 139 |
| Mauna Loa, HI, United States | 19.53 | 0.57692 | 0.35833 | 0.50906 | 0.04962 | 10.25995 | <0.0001 | 7.88426 | 213 |
| Reunion Island, St. Denis, France | -20.90 | 0.29475 | -0.01221 | 0.23706 | 0.09532 | 2.48686 | 0.01546 | 6.27246 | 67 |
| Alice Springs, Australia | -23.80 | 0.59268 | -0.13242 | 0.60587 | 0.0691 | 8.7686 | <0.0001 | 6.67145 | 144 |
| Lauder, New Zealand | -45.04 | 0.52901 | 0.08797 | 0.84026 | 0.09301 | 9.03374 | <0.0001 | 13.34001 | 212 |
| Ushuaia, Argentina | -54.82 | 0.44285 | -0.63202 | 0.79185 | 0.21234 | 3.72909 | 4.44141E-4 | 21.80721 | 59 |
| Palmer, Antarctica | -64.77 | 0.4665 | -0.09991 | 0.71651 | 0.12103 | 5.92008 | <0.0001 | 30.58139 | 128 |
| Arrival Heights, Antarctica | -77.83 | 0.93868 | 0.53114 | 0.99985 | 0.03298 | 30.31727 | <0.0001 | 10.4058 | 126 |
| South Pole, Antarctica | -90 | 0.94832 | -0.20478 | 1.04666 | 0.03238 | 32.32625 | <0.0001 | 9.1413 | 119 |

**Table S2. (a)** Correlation results between model simulations (HIS-SD) and satellite SBUV (v8.7) total ozone data for the northern high latitude zonal mean (55º–75º N), the southern high latitude zonal mean (55º–75º S), and the near global mean (50º N–50º S). **(b)** Same as (a) but for the HIS-SD simulation and satellite MODIS/Terra cloud fraction data.

| **(a) Total ozone** | | | | | | | |
|---|---|---|---|---|---|---|---|
| | R | Slope | Error | t-value | p-value | N | RMSE |
| 55º–75º N | 0.86224 | 0.77653 | 0.04016 | 19.33488 | <0.0001 | 131 | 1.05561 |
| 55º–75º S | 0.94715 | 0.88849 | 0.0267 | 33.27424 | <0.0001 | 129 | 1.6596 |
| 50º N – 50º S | 0.84183 | 0.74437 | 0.0321 | 23.18663 | <0.0001 | 223 | 0.36078 |
| **(b) Cloud cover** | | | | | | | |
| | R | Slope | Error | t-value | p-value | N | RMSE |
| 55º–75º N | 0.46665 | 0.30604 | 0.05107 | 5.9926 | <0.0001 | 131 | 1.20808 |
| 55º–75º S | 0.49435 | 0.59751 | 0.0936 | 6.38356 | <0.0001 | 128 | 1.04528 |
| 50º N – 50º S | 0.40141 | 0.51432 | 0.07912 | 6.5005 | <0.0001 | 222 | 1.07126 |

**Table S3.** Statistics of correlations between simulated (EMAC CCM "specified dynamics" simulation SC1SD-base-02, referred as HIS-SD) and observed (satellite SBUV v8.7) total ozone data after removing variability related to the seasonal cycle. Stations are listed from north to south.

| Station | Latitude | Correlation | Intercept (%) | Slope | Error | t-value | p-value | RMSE | N |
|---|---|---|---|---|---|---|---|---|---|
| Summit, Greenland | 72.58 | 0.92746 | 0.02356 | 0.79136 | 0.02809 | 28.17083 | <0.0001 | 1.49119 | 131 |
| Barrow, AK, United States | 71.32 | 0.91395 | -0.07433 | 0.89544 | 0.03501 | 25.57902 | <0.0001 | 1.51872 | 131 |
| Sodankylä, Finland | 67.37 | 0.91871 | 0.04423 | 0.83244 | 0.03151 | 26.42107 | <0.0001 | 1.58014 | 131 |
| Villeneuve d'Ascq, France | 50.61 | 0.9327 | 0.00865 | 0.8832 | 0.02297 | 38.44502 | <0.0001 | 1.46157 | 223 |
| Groß-Enzersdorf, Austria | 48.20 | 0.90117 | -2.71279E-4 | 0.83541 | 0.02703 | 30.90677 | <0.0001 | 1.49264 | 223 |
| Zugspitze, Germany | 47.42 | 0.90637 | -0.00303 | 0.81468 | 0.02554 | 31.89276 | <0.0001 | 1.41823 | 223 |
| Hoher Sonnblick, Austria | 47.05 | 0.90234 | -0.00193 | 0.80291 | 0.0258 | 31.12256 | <0.0001 | 1.41626 | 223 |
| Aosta, Italy | 45.74 | 0.90909 | -0.00663 | 0.85712 | 0.02642 | 32.44056 | <0.0001 | 1.43109 | 223 |
| Observatoire de Haute Provence, France | 43.94 | 0.90651 | -0.01346 | 0.86718 | 0.02717 | 31.9194 | <0.0001 | 1.38784 | 223 |
| Thessaloniki, Greece | 40.63 | 0.84905 | -0.00866 | 0.79992 | 0.03348 | 23.89163 | <0.0001 | 1.42528 | 223 |
| Boulder, CO, United States | 39.99 | 0.85389 | -0.00778 | 0.75677 | 0.03103 | 24.38992 | <0.0001 | 1.46848 | 223 |
| Athens, Greece | 37.99 | 0.84712 | -0.01027 | 0.84485 | 0.03565 | 23.69841 | <0.0001 | 1.4082 | 223 |
| Mauna Loa, HI, United States | 19.53 | 0.85221 | -0.05717 | 0.94063 | 0.03885 | 24.21468 | <0.0001 | 1.40913 | 223 |
| Reunion Island, St. Denis, France | -20.90 | 0.76869 | 0.00266 | 0.80808 | 0.04523 | 17.8657 | <0.0001 | 1.34564 | 223 |
| Alice Springs, Australia | -23.80 | 0.85137 | 0.00285 | 0.85687 | 0.03551 | 24.12727 | <0.0001 | 1.28936 | 223 |
| Lauder, New Zealand | -45.04 | 0.92117 | 0.03962 | 0.87216 | 0.02479 | 35.18816 | <0.0001 | 1.16087 | 223 |
| Ushuaia, Argentina | -54.82 | 0.96269 | 0.01129 | 0.86996 | 0.02179 | 39.93037 | <0.0001 | 1.27243 | 128 |
| Palmer, Antarctica | -64.77 | 0.95377 | -0.10395 | 0.89986 | 0.02526 | 35.6213 | <0.0001 | 2.48476 | 128 |
| Arrival Heights, Antarctica | -77.83 | 0.89556 | -0.13406 | 0.65541 | 0.02901 | 22.59306 | <0.0001 | 5.36836 | 128 |
| South Pole, Antarctica | -90 | no data | no data | no data | no data | no data | no data | no data | no data |

**Table S4.** Statistics of correlations between simulated (EMAC CCM "specified dynamics" simulation SC1SD-base-02, referred as HIS-SD) and observed (satellite MODIS/Terra) cloudiness data after removing variability related to the seasonal cycle. Stations are listed from north to south.

| Station | Latitude | Correlation | Intercept (%) | Slope | Error | t-value | p-value | RMSE | N |
|---|---|---|---|---|---|---|---|---|---|
| Summit, Greenland | 72.58 | 0.19614 | 0.01033 | 0.06936 | 0.03053 | 2.2719 | 0.02475 | 5.84144 | 131 |
| Barrow, AK, United States | 71.32 | 0.59746 | 0.01835 | 0.75521 | 0.08925 | 8.46216 | <0.0001 | 11.01167 | 131 |
| Sodankylä, Finland | 67.37 | 0.53468 | -0.01445 | 0.26193 | 0.03645 | 7.18618 | <0.0001 | 4.15905 | 131 |
| Villeneuve d'Ascq, France | 50.61 | 0.5155 | -0.0936 | 0.50165 | 0.05622 | 8.92306 | <0.0001 | 9.15062 | 222 |
| Groß-Enzersdorf, Austria | 48.20 | 0.65362 | -0.15377 | 0.61759 | 0.04821 | 12.80986 | <0.0001 | 10.16946 | 222 |
| Zugspitze, Germany | 47.42 | 0.54779 | -0.02613 | 0.57172 | 0.05887 | 9.71188 | <0.0001 | 11.86551 | 222 |
| Hoher Sonnblick, Austria | 47.05 | 0.55629 | -0.04129 | 0.61867 | 0.06231 | 9.92925 | <0.0001 | 12.71143 | 222 |
| Aosta, Italy | 45.74 | 0.66827 | -0.06953 | 0.68816 | 0.05165 | 13.3242 | <0.0001 | 10.39675 | 222 |
| Observatoire de Haute Provence, France | 43.94 | 0.44998 | -0.07471 | 0.45353 | 0.06068 | 7.4736 | <0.0001 | 13.98316 | 222 |
| Thessaloniki, Greece | 40.63 | 0.64131 | -0.8916 | 0.86816 | 0.07084 | 12.2556 | <0.0001 | 20.59386 | 217 |
| Boulder, CO, United States | 39.99 | 0.53923 | -0.09291 | 0.48194 | 0.05075 | 9.49717 | <0.0001 | 11.54097 | 222 |
| Athens, Greece | 37.99 | 0.48522 | -1.26658 | 0.68926 | 0.08592 | 8.02237 | <0.0001 | 26.07997 | 211 |
| Mauna Loa, HI, United States | 19.53 | 0.592 | -1.20988 | 1.35496 | 0.1258 | 10.77071 | <0.0001 | 26.90733 | 217 |
| Reunion Island, St. Denis, France | -20.90 | 0.52781 | -1.53877 | 1.18482 | 0.12943 | 9.15397 | <0.0001 | 26.36888 | 219 |
| Alice Springs, Australia | -23.80 | 0.62268 | -0.25621 | 0.58451 | 0.05233 | 11.16931 | <0.0001 | 26.82549 | 199 |
| Lauder, New Zealand | -45.04 | 0.3935 | 0.07335 | 0.45073 | 0.071 | 6.34872 | <0.0001 | 8.34939 | 222 |
| Ushuaia, Argentina | -54.82 | 0.44364 | -0.09417 | 0.60317 | 0.10855 | 5.55661 | <0.0001 | 5.2374 | 128 |
| Palmer, Antarctica | -64.77 | 0.47323 | 0.00415 | 0.55019 | 0.09124 | 6.02995 | <0.0001 | 3.95994 | 128 |
| Arrival Heights, Antarctica | -77.83 | 0.53671 | 0.28879 | 0.94892 | 0.1329 | 7.14 | <0.0001 | 15.21939 | 129 |
| South Pole, Antarctica | -90 | -0.17482 | -0.14172 | -0.04717 | 0.02467 | -1.91231 | 0.0583 | 8.61534 | 118 |

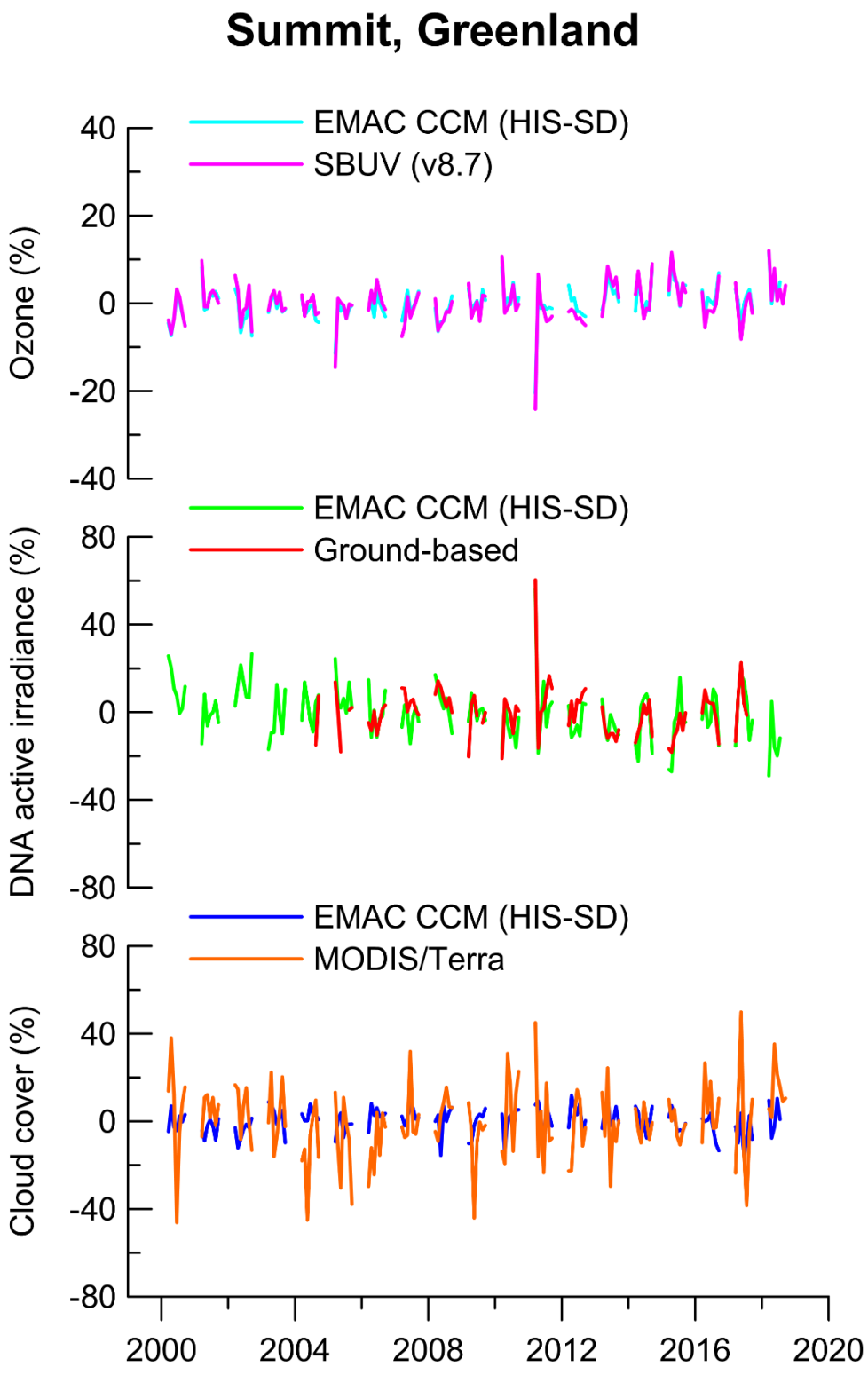


**Figure S5.** Time series of ozone, DNA active irradiance, and cloud cover at **Summit, Greenland**, after removing variability related to the seasonal cycle.

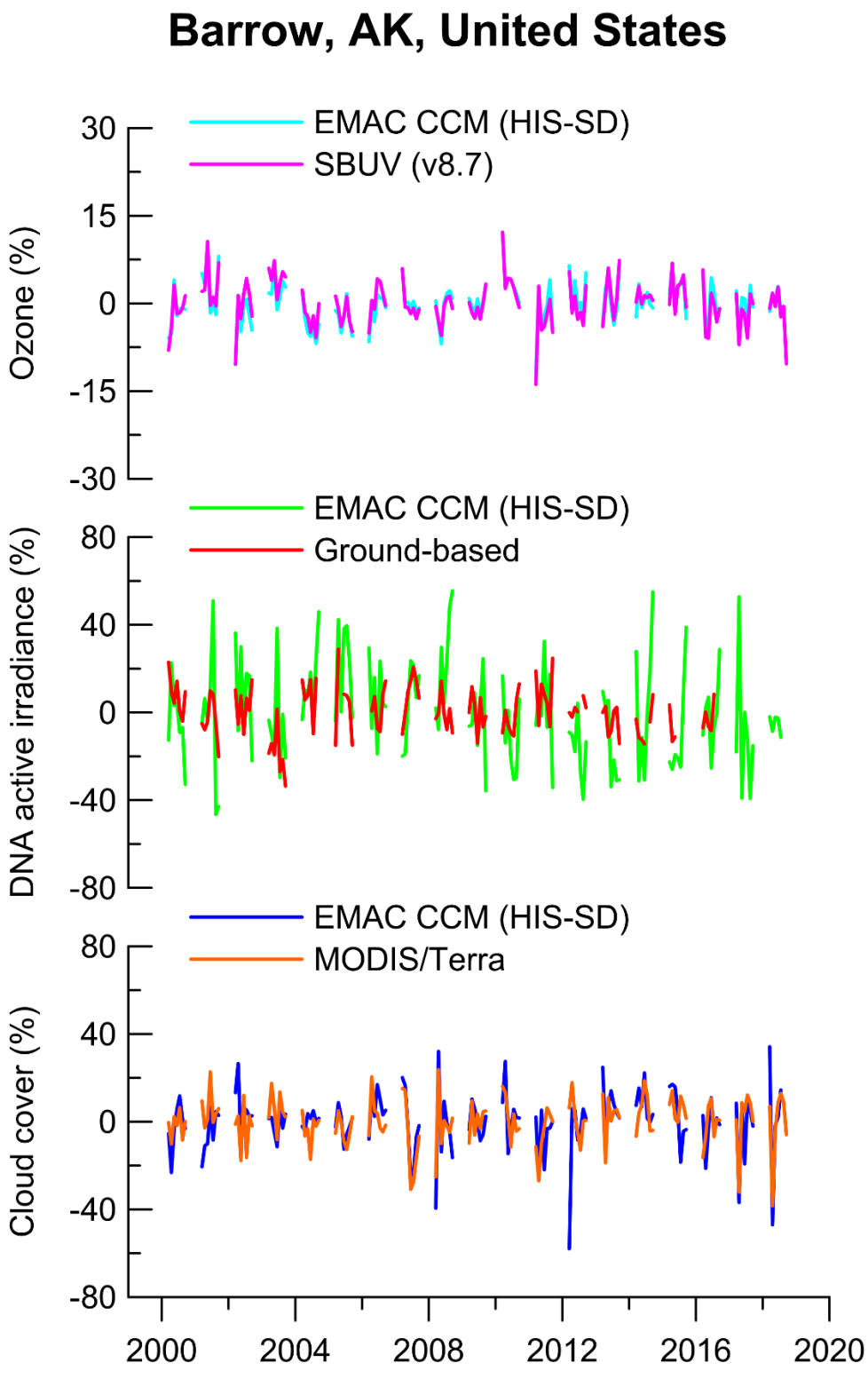


**Figure S6.** Same as Figure S5 but for **Barrow, AK, United States.**

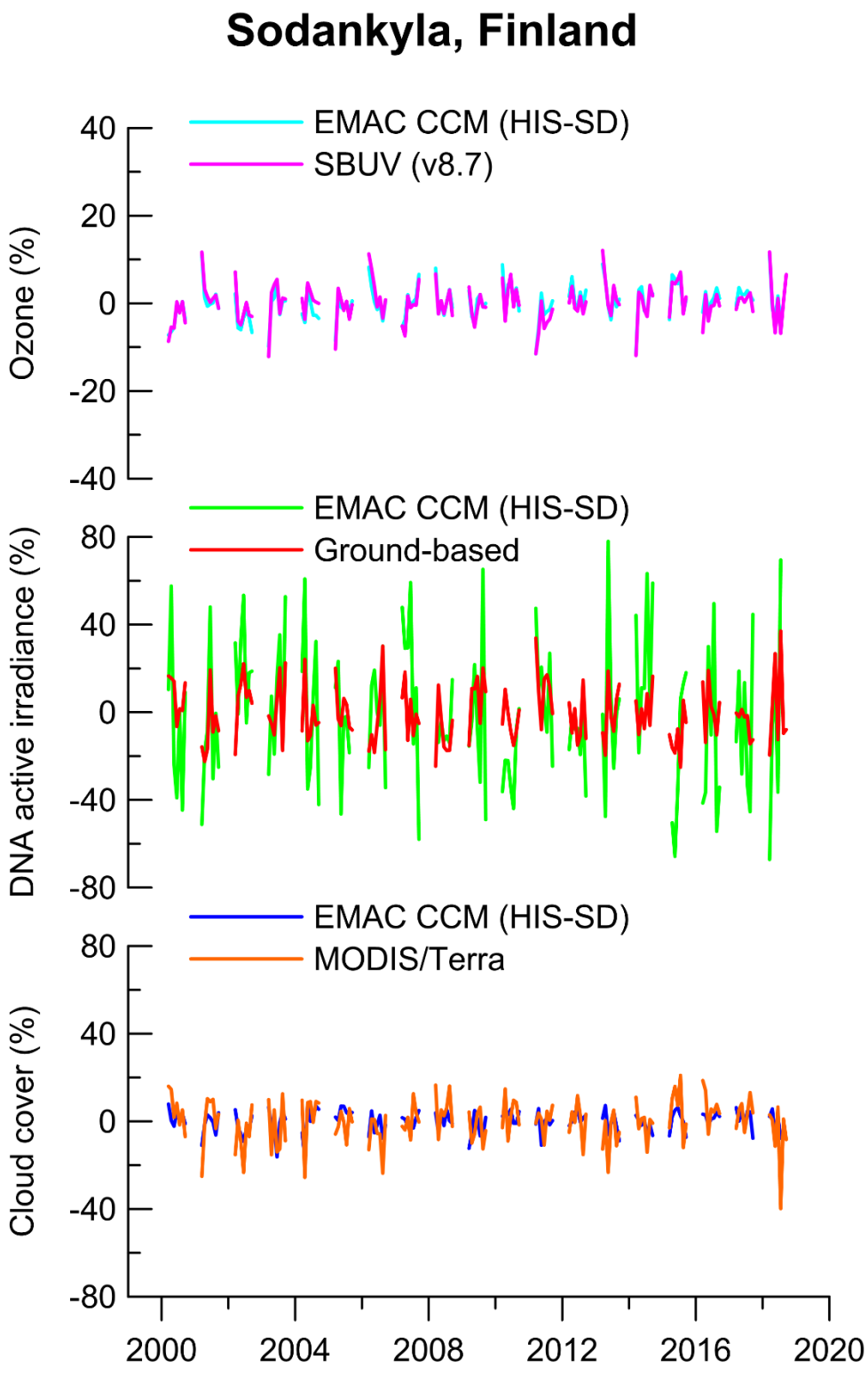


**Figure S7.** Same as Figure S5 but for **Sodankylä, Finland.**

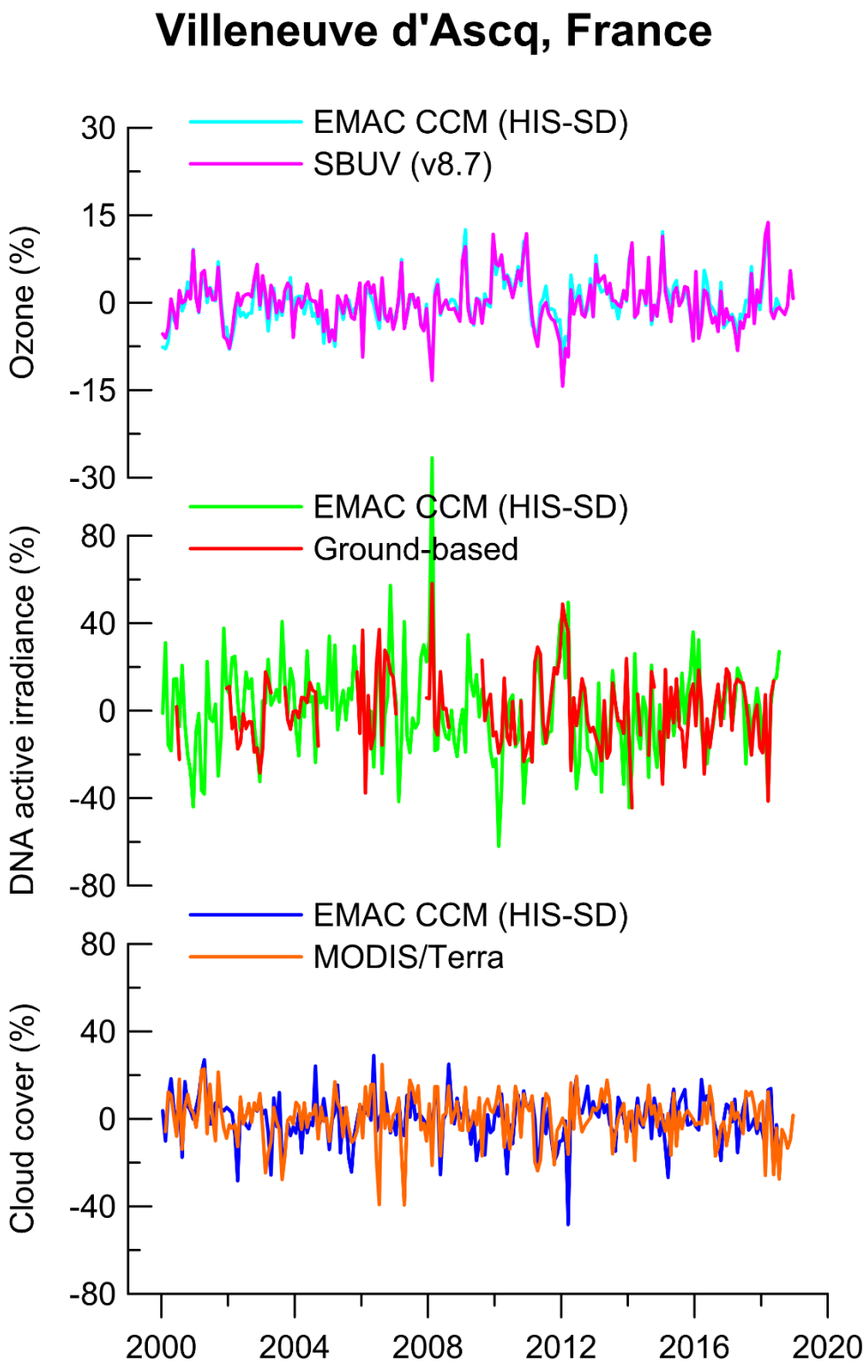


**Figure S8.** Same as Figure S5 but for **Villeneuve d'Ascq, France.**

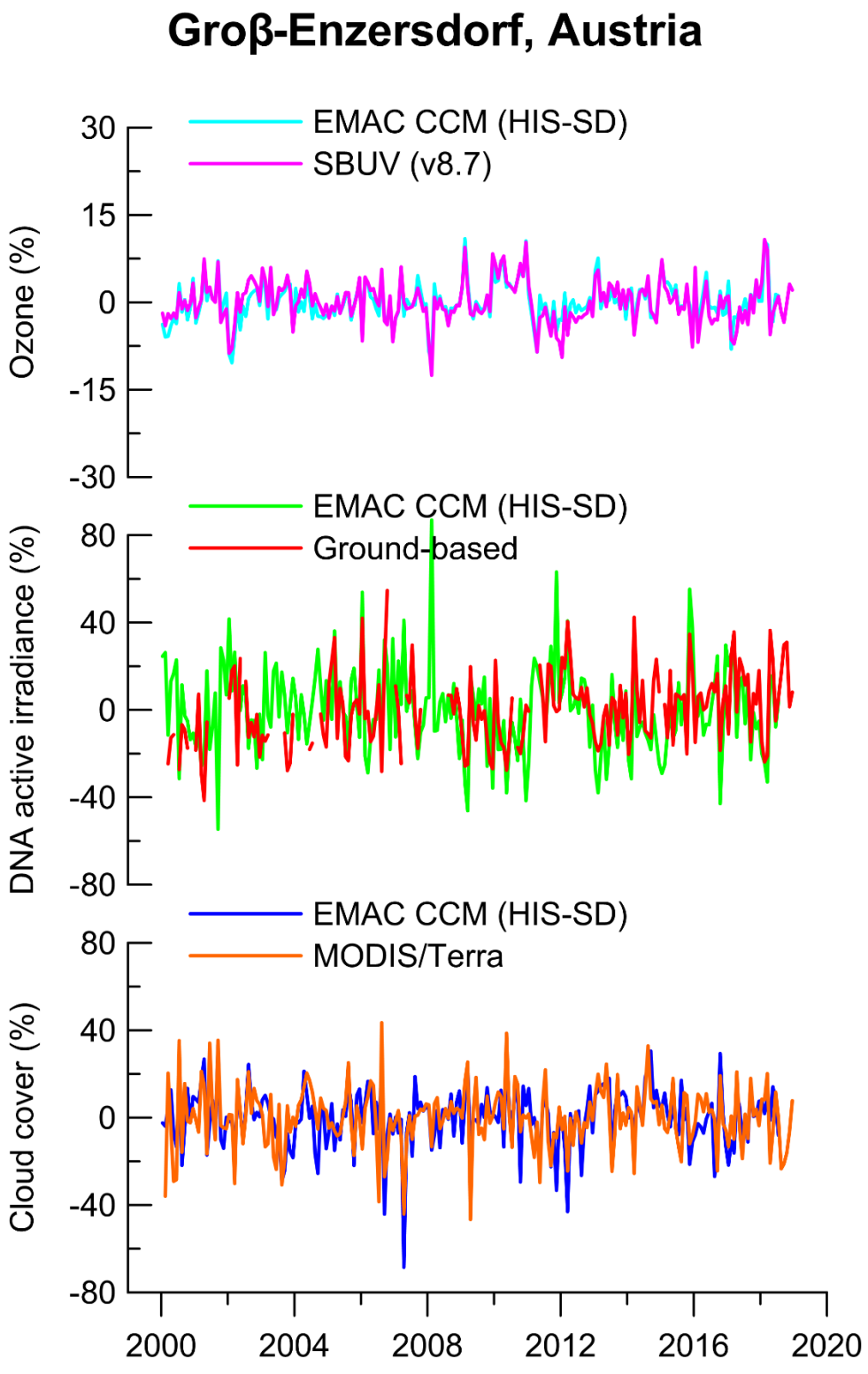


**Figure S9.** Same as Figure S5 but for **Groß-Enzersdorf, Austria.**

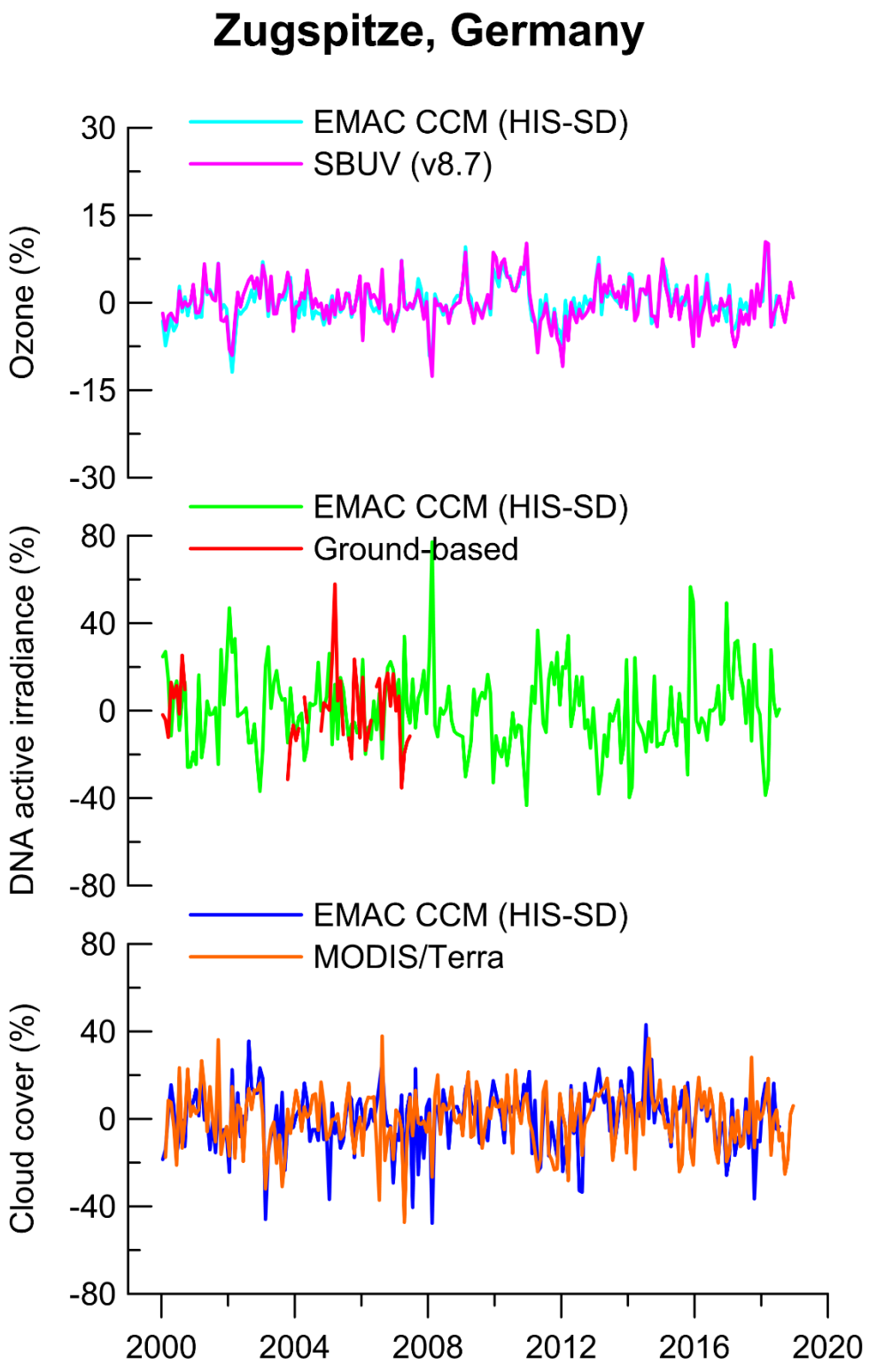


**Figure S10.** Same as Figure S5 but for **Zugspitze, Germany.**

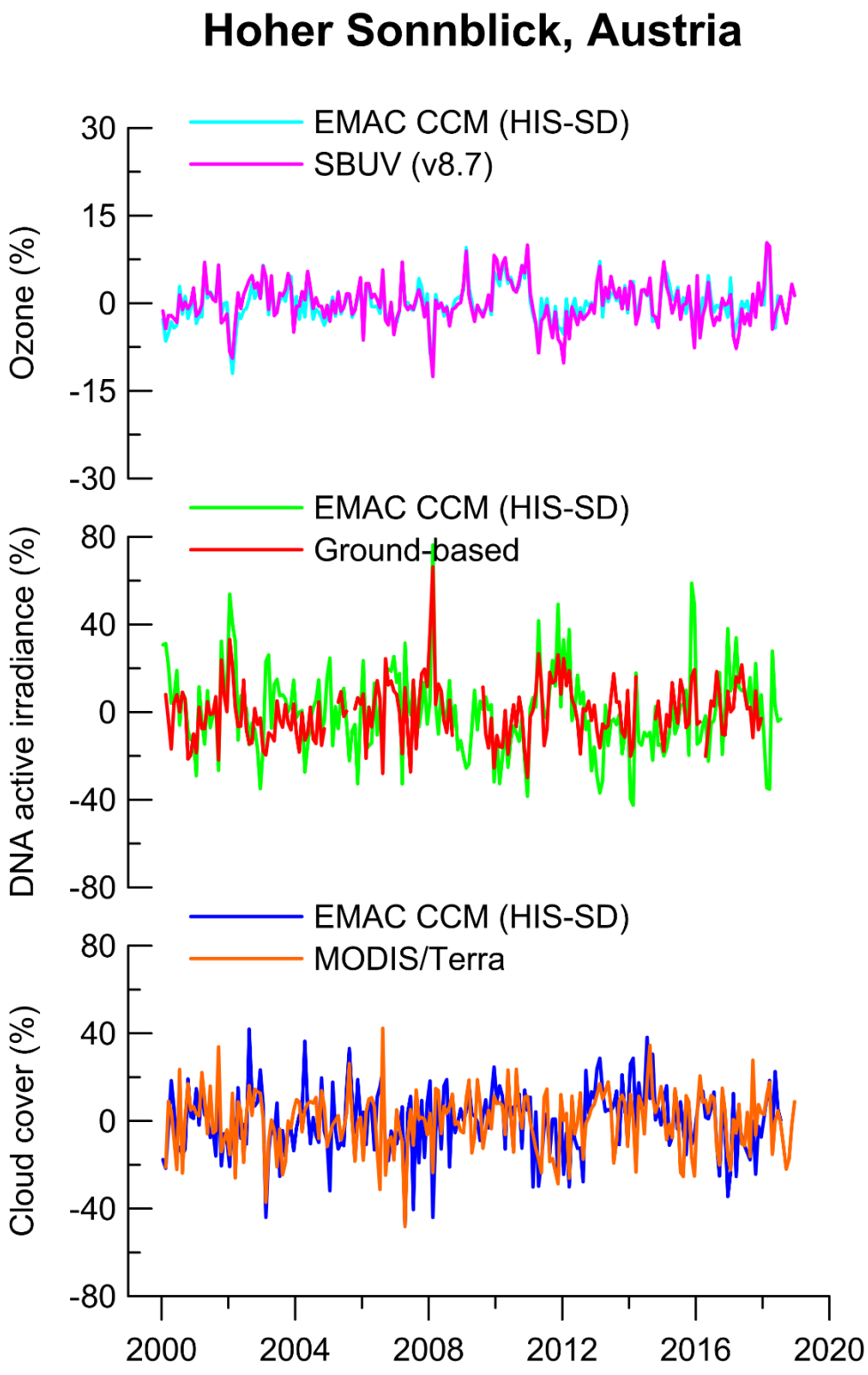


**Figure S11.** Same as Figure S5 but for **Hoher Sonnblick, Austria.**

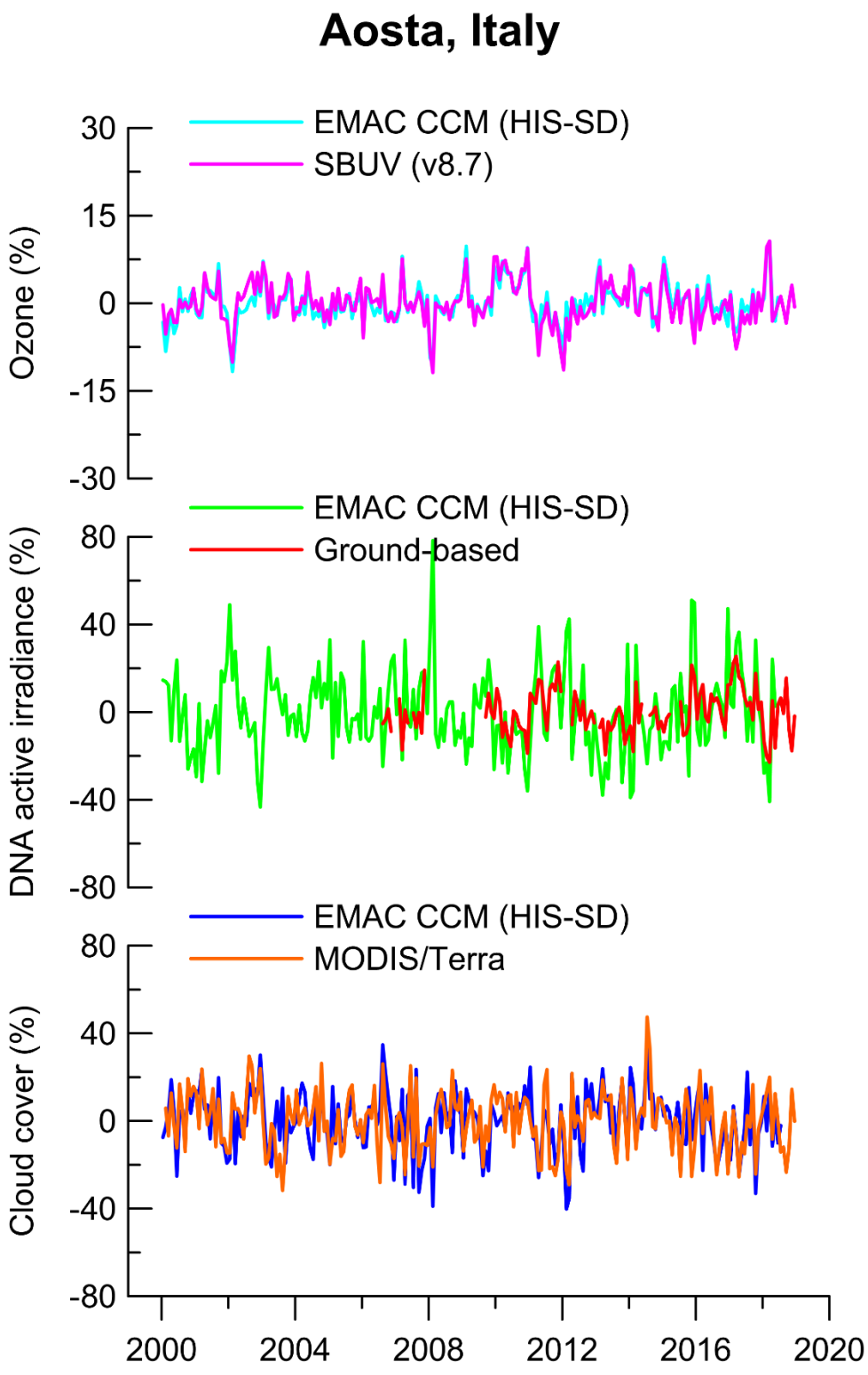


**Figure S12.** Same as Figure S5 but for **Aosta, Italy.**

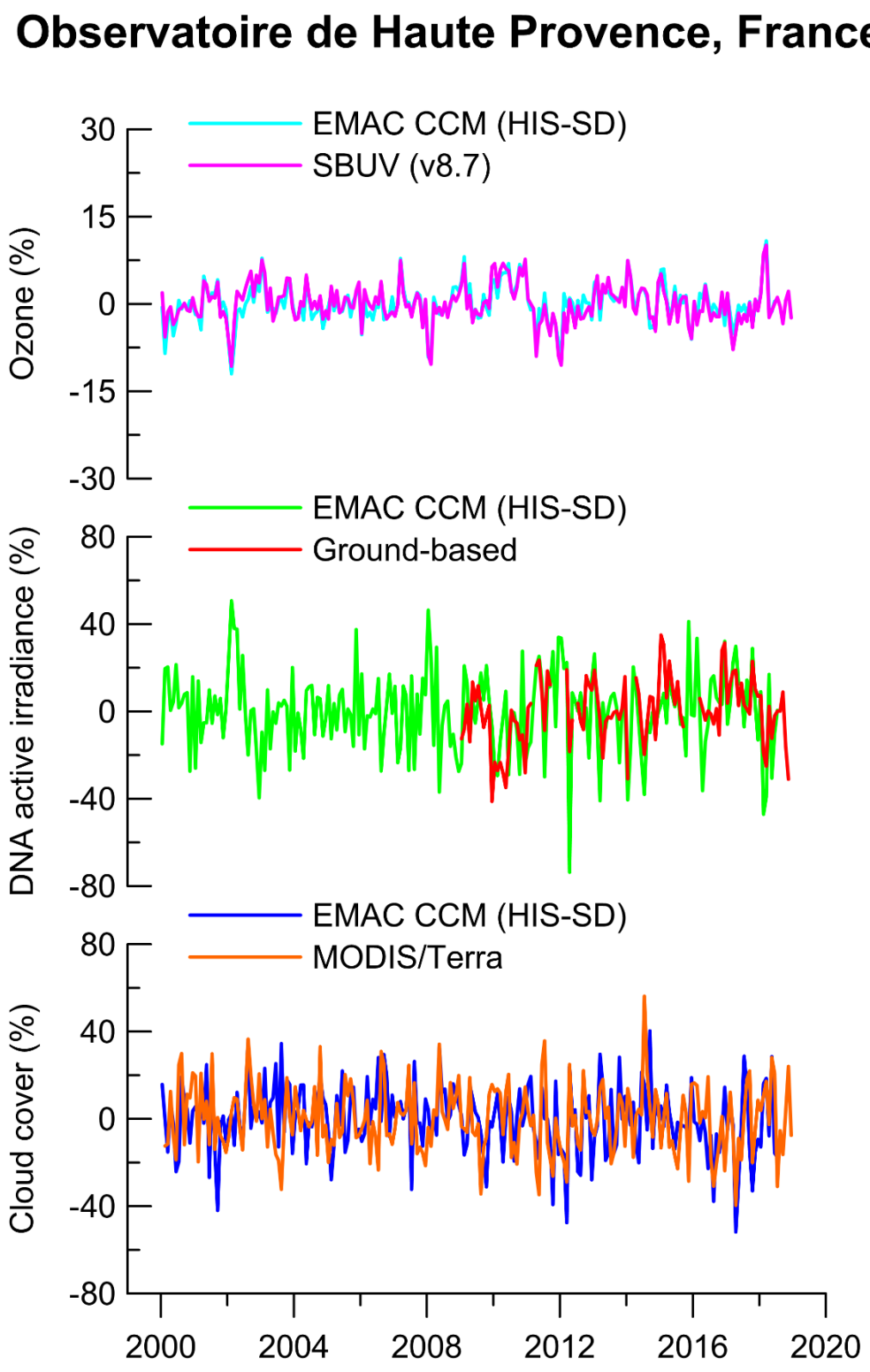


**Figure S13.** Same as Figure S5 but for **Observatoire de Haute Provence, France.**

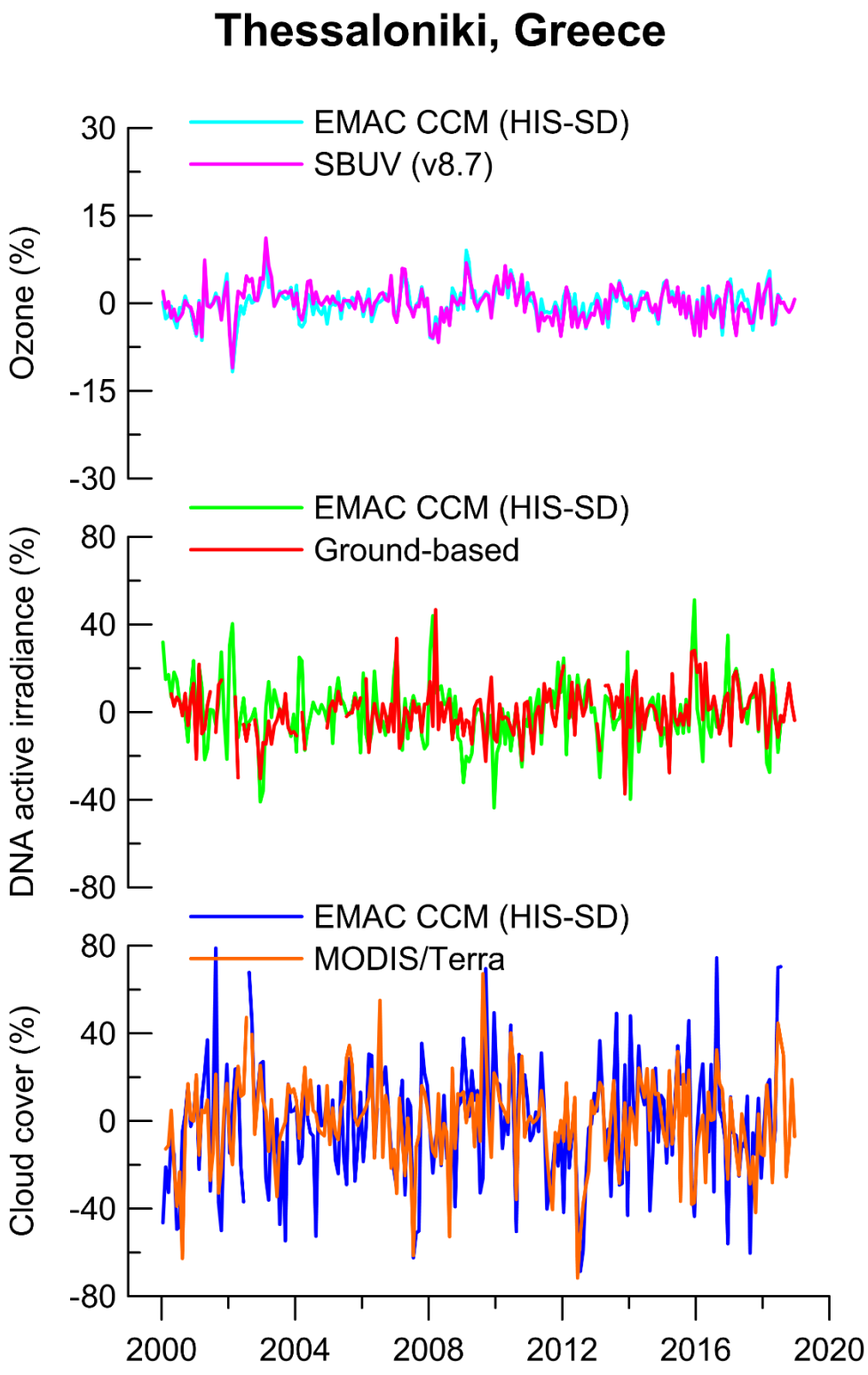


**Figure S14.** Same as Figure S5 but for **Thessaloniki, Greece.**

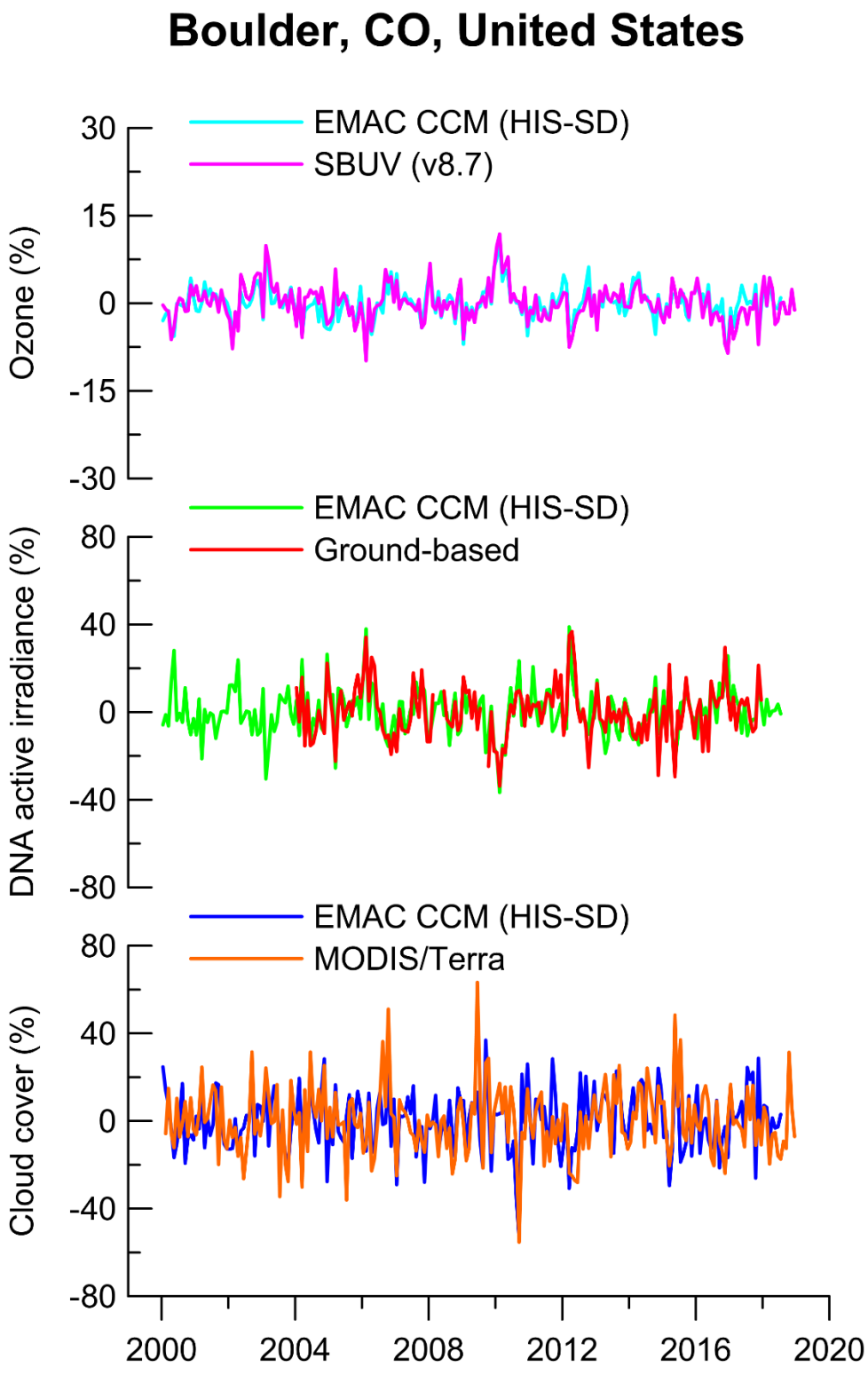


**Figure S15.** Same as Figure S5 but for **Boulder, CO, United States.**

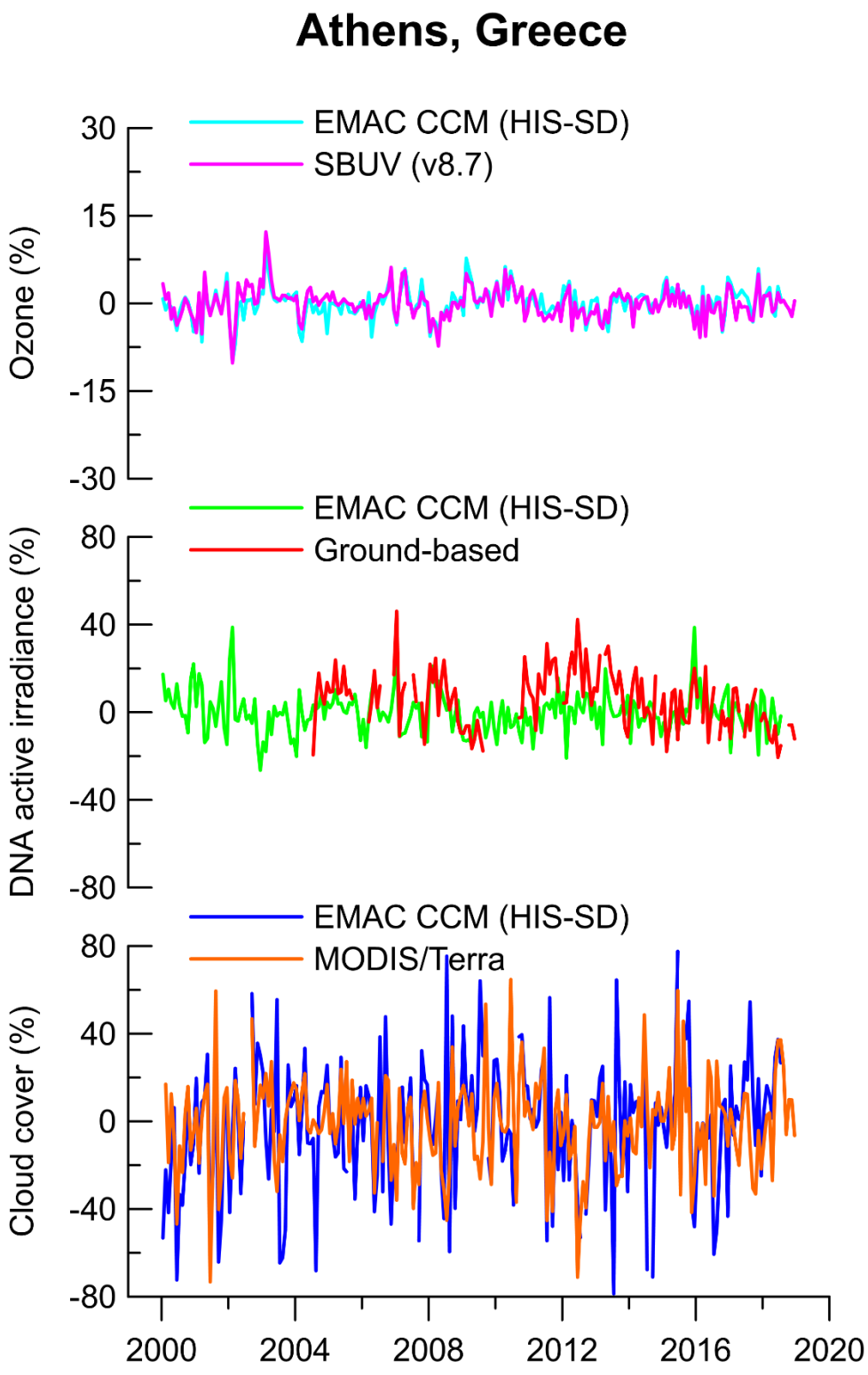


**Figure S16.** Same as Figure S5 but for **Athens, Greece.**

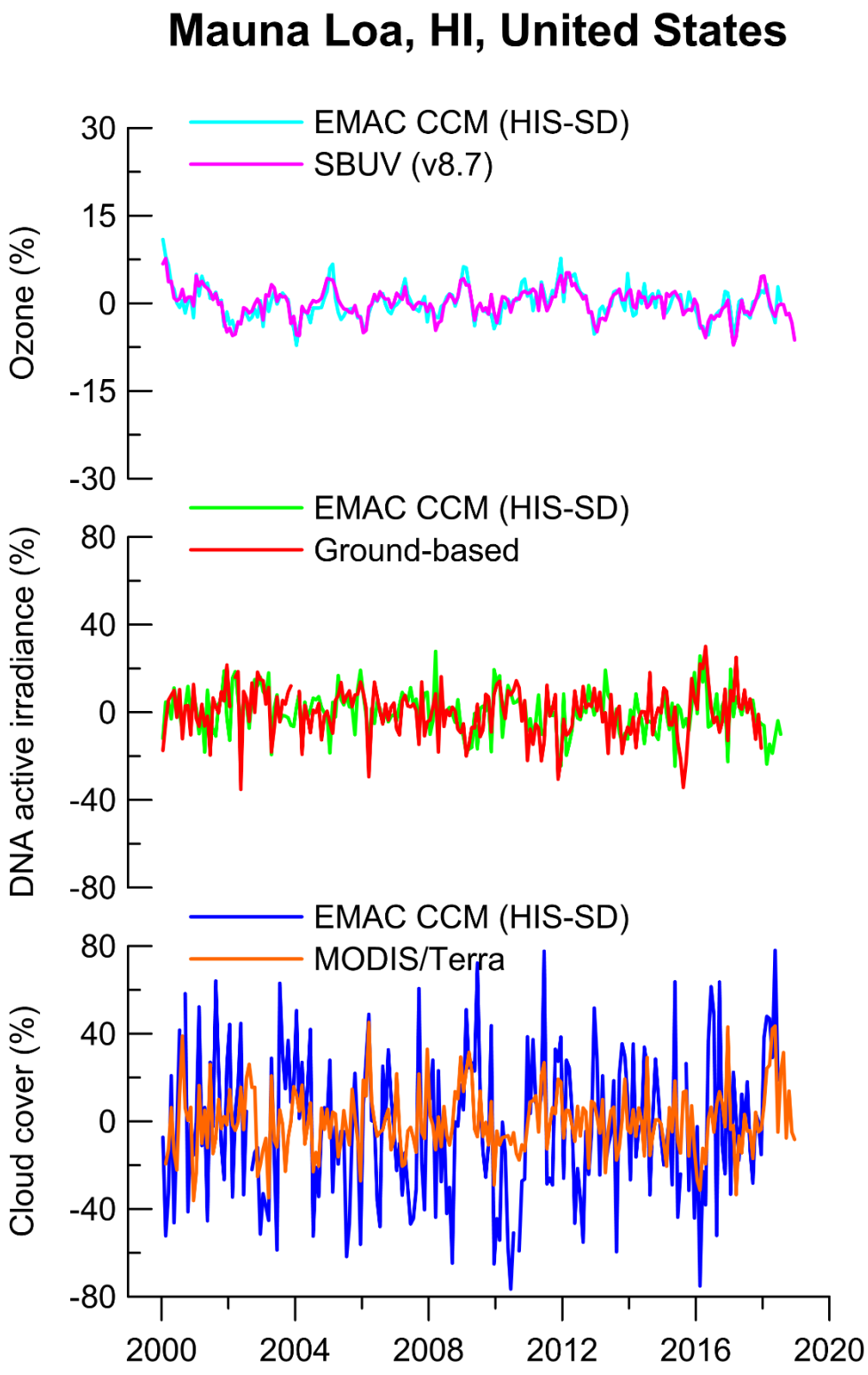


**Figure S17.** Same as Figure S5 but for **Mauna Loa, HI, United States.**

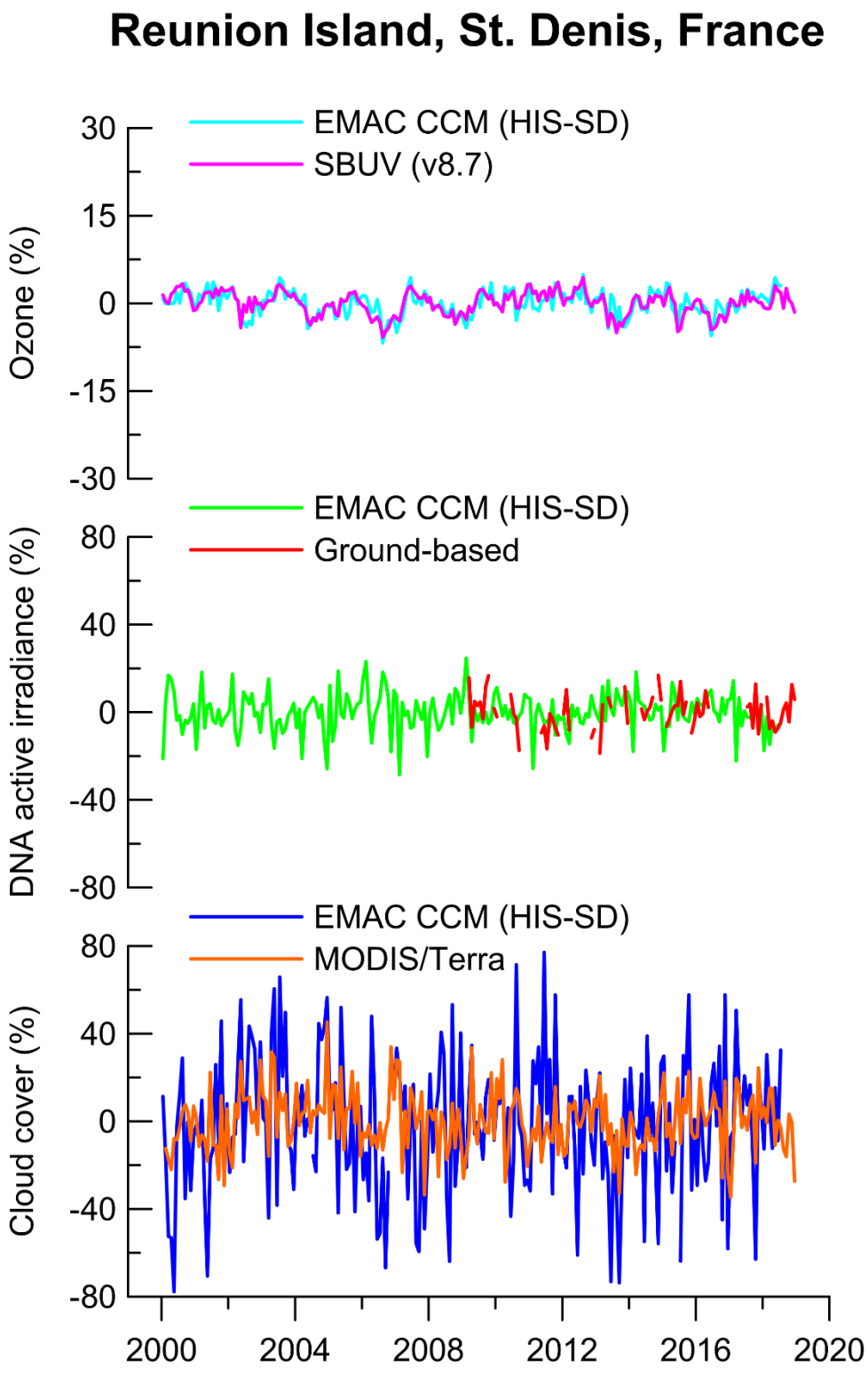


**Figure S18.** Same as Figure S5 but for **Reunion Island, St. Denis, France.**

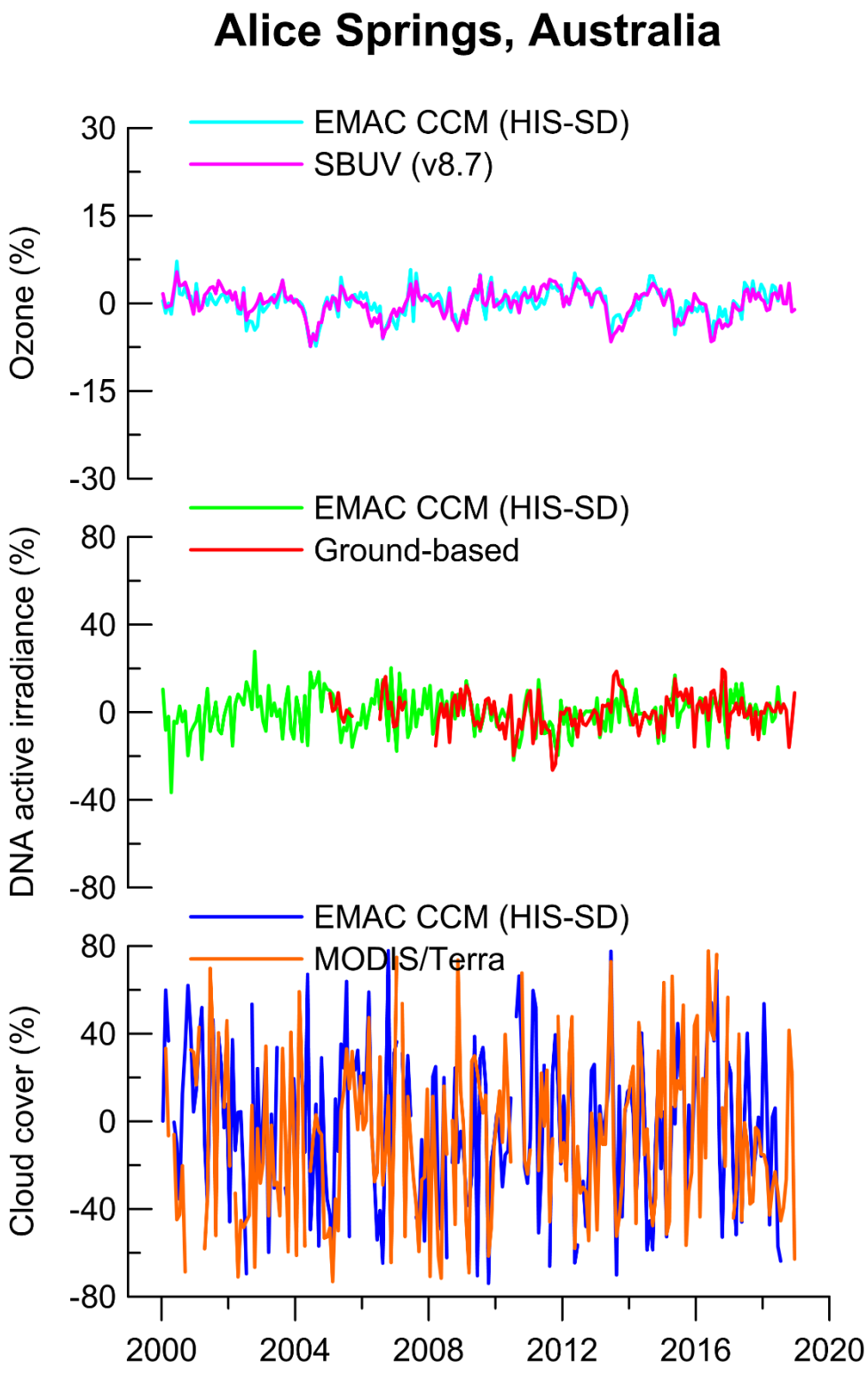


**Figure S19.** Same as Figure S5 but for **Alice Springs, Australia.**

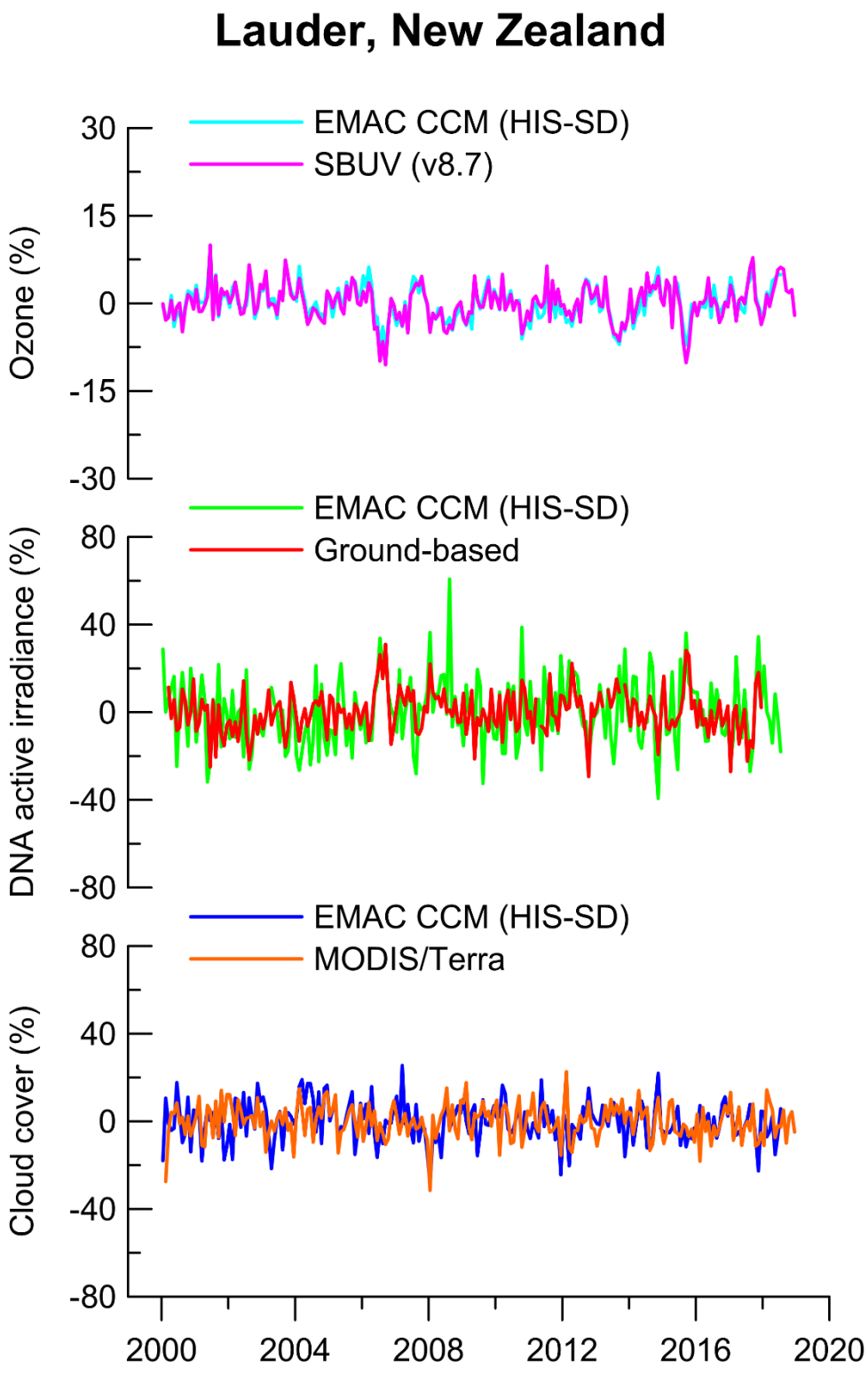


**Figure S20.** Same as Figure S5 but for **Lauder, New Zealand.**

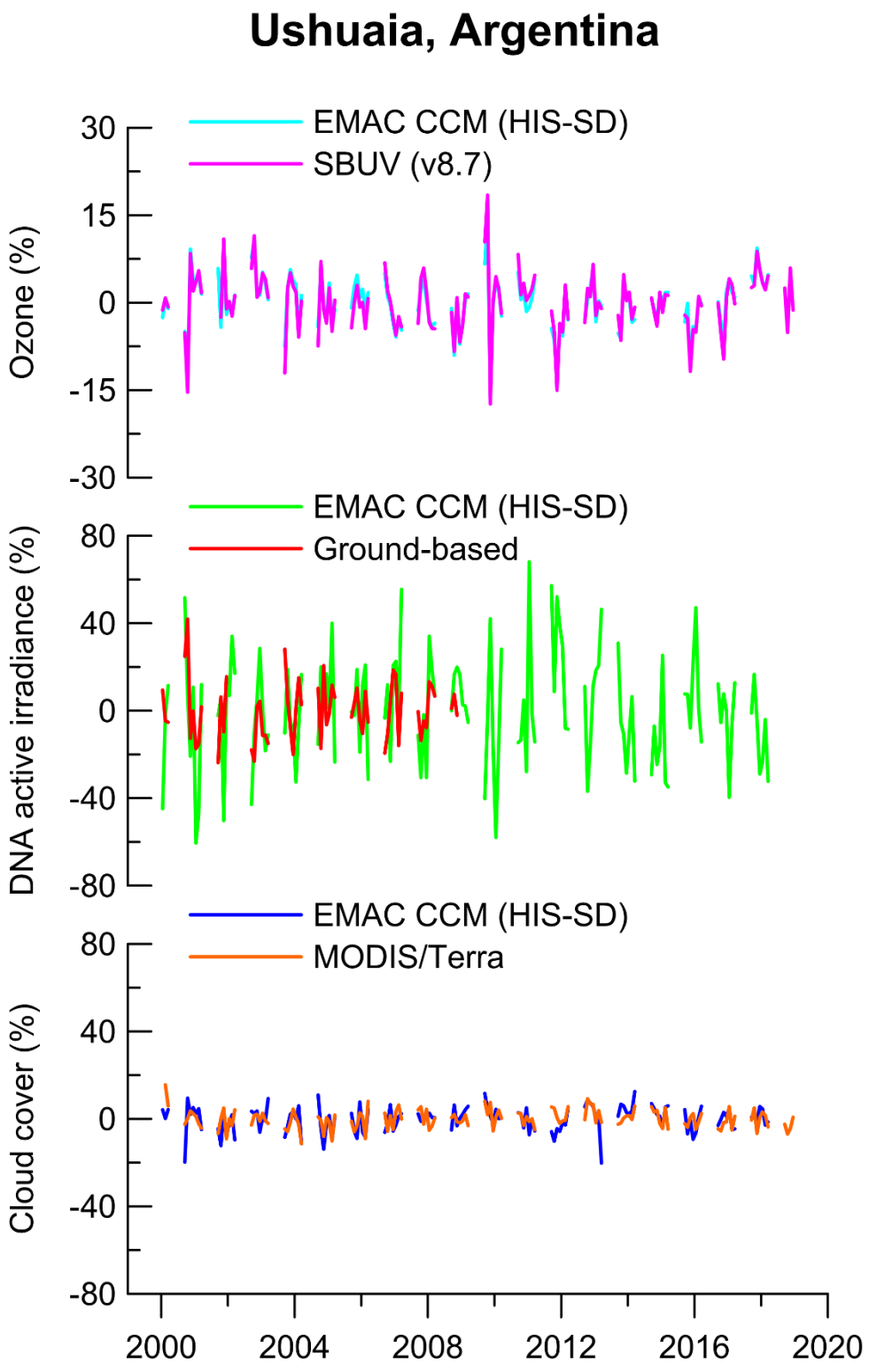


**Figure S21.** Same as Figure S5 but for **Ushuaia, Argentina.**

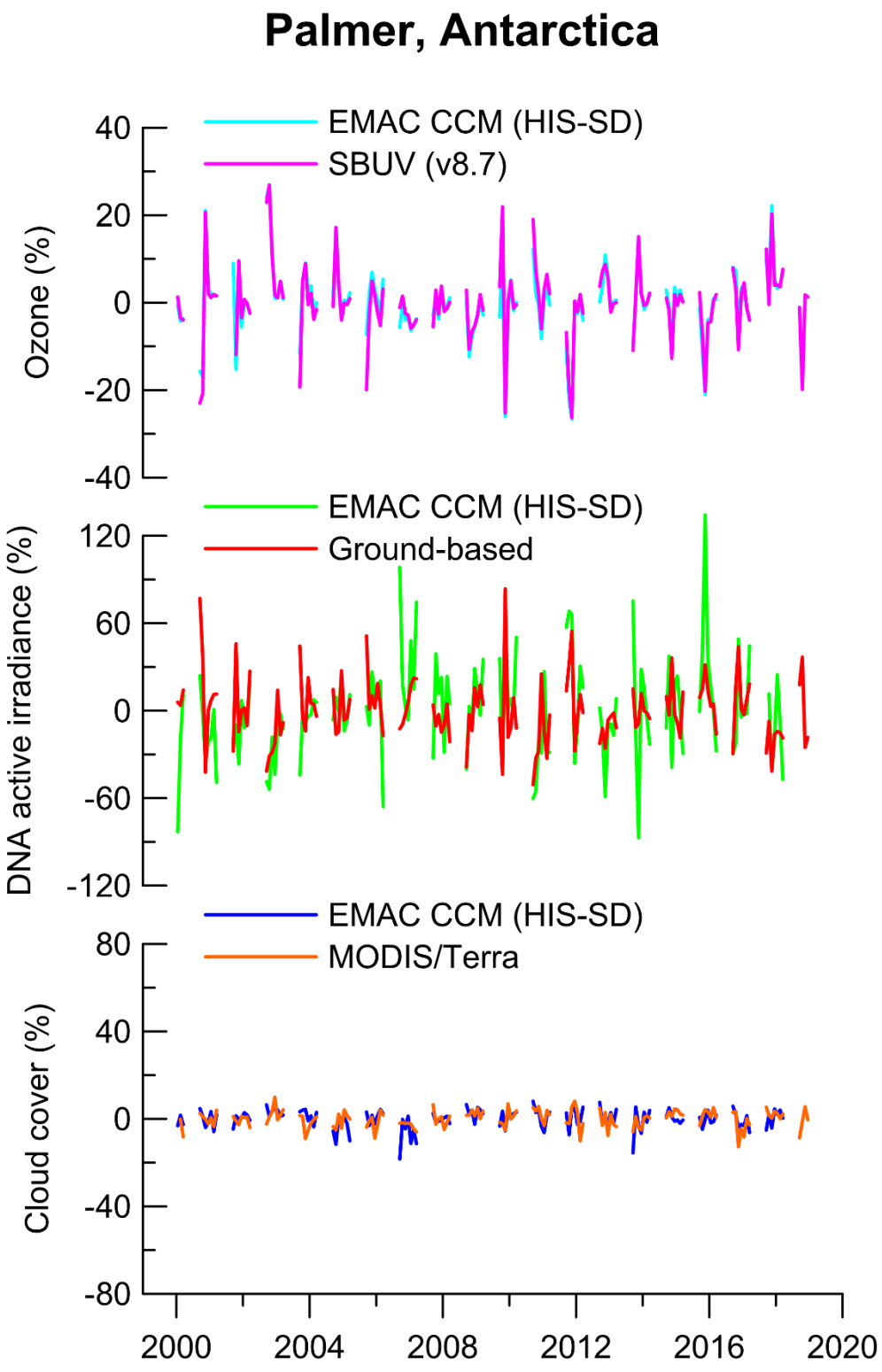


**Figure S22.** Same as Figure S5 but for **Palmer, Antarctica.**

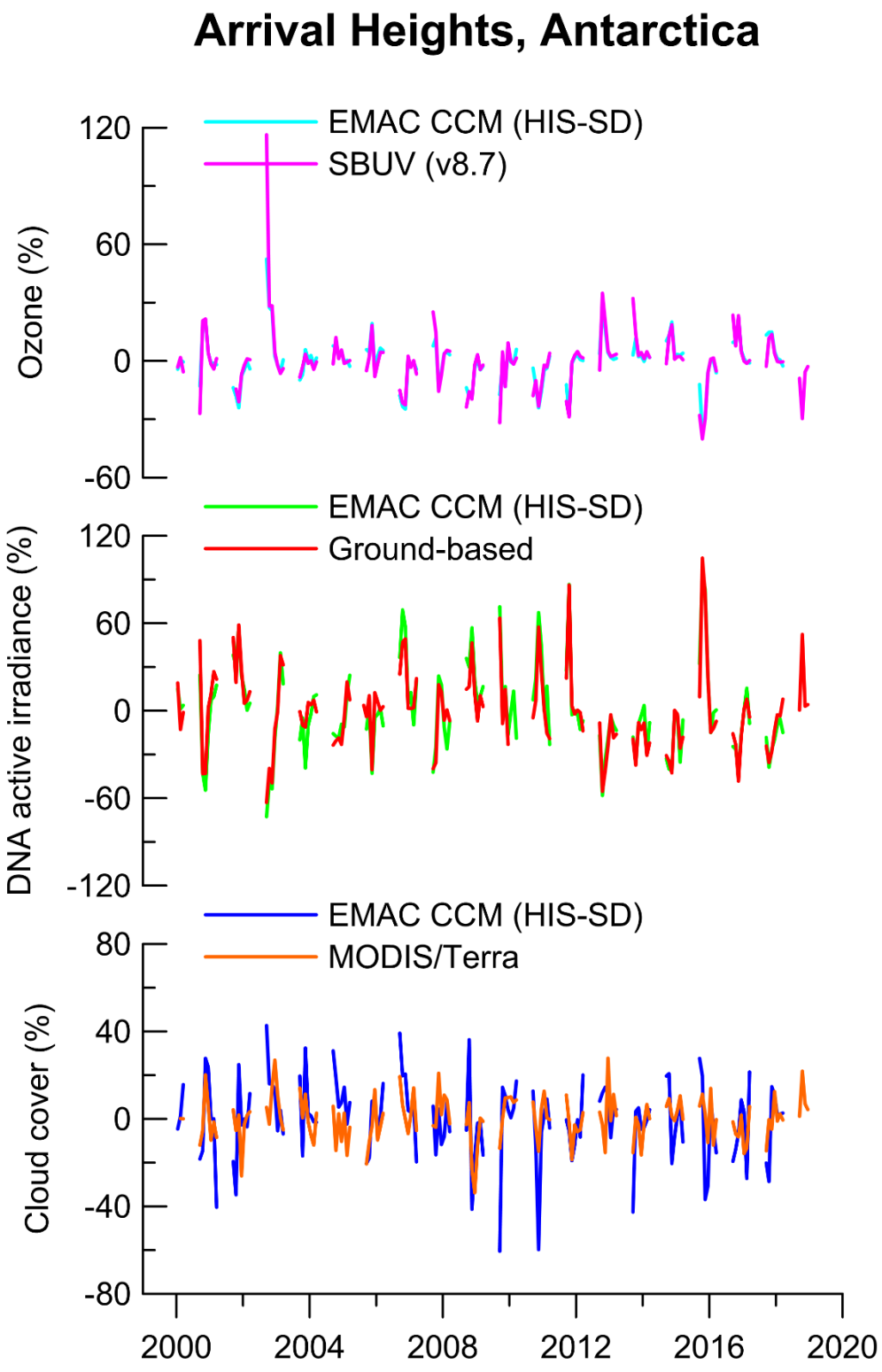


**Figure S23.** Same as Figure S5 but for **Arrival Heights, Antarctica.**

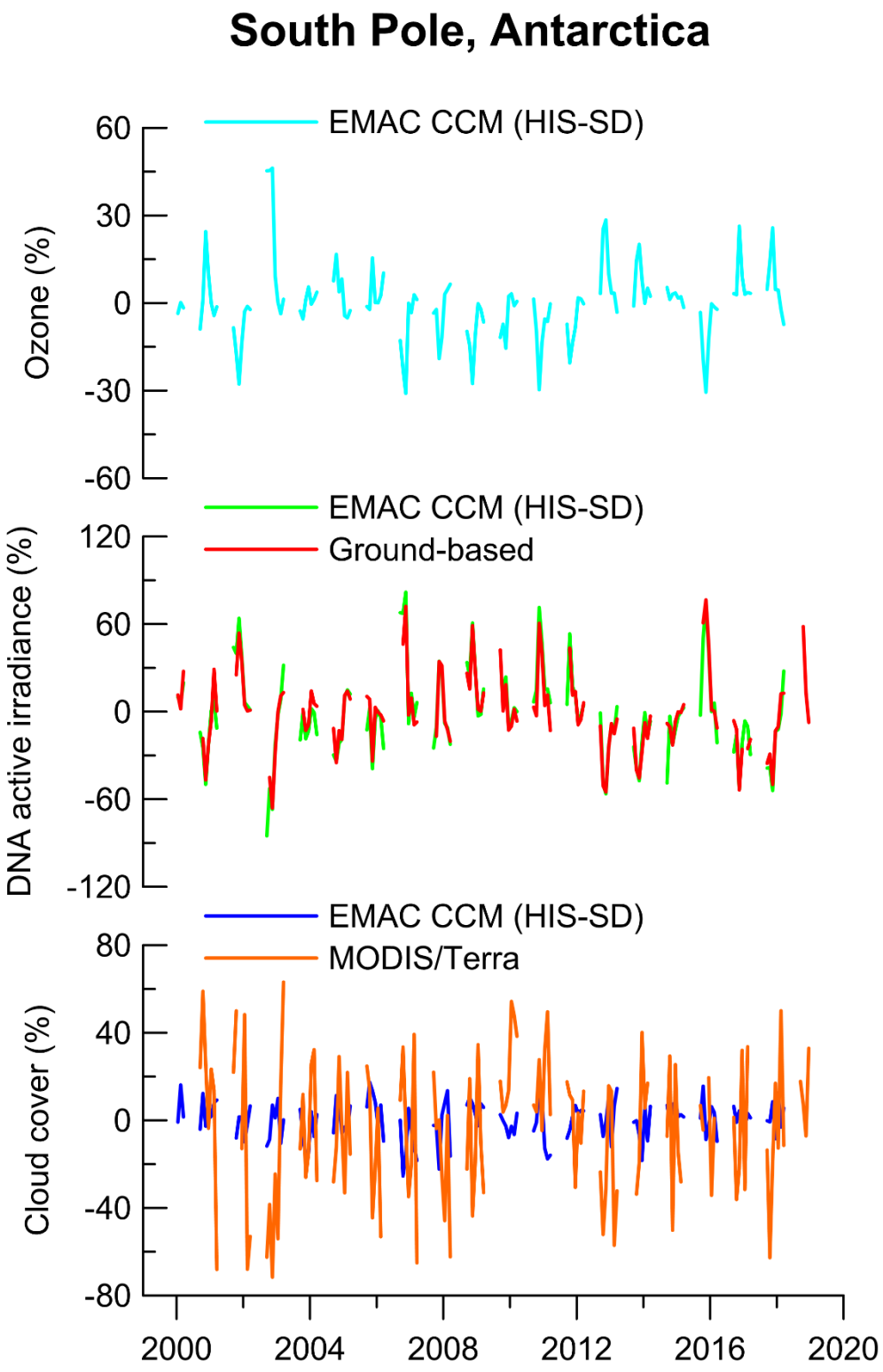


**Figure S24.** Same as Figure S5 but for **South Pole, Antarctica.**